Journal of Alloys and Compounds 662 (2016) 516–527

Contents lists available at ScienceDirect

Journal of Alloys and Compounds

journal homepage: http://www.elsevier.com/locate/jalcom

CdS/Cu_2S co-sensitized TiO_2 branched nanorod arrays of enhanced photoelectrochemical properties by forming nanoscale heterostructure

Lin Tang [a, b, *], Yaocheng Deng [a, b], Guangming Zeng [a, b, **], Wei Hu [c], Jiajia Wang [a, b], Yaoyu Zhou [a, b], Jingjing Wang [a, b], Jing Tang [a, b], Wei Fang [a, b]

[a] College of Environmental Science and Engineering, Hunan University, Changsha, 410082, China
[b] Key Laboratory of Environmental Biology and Pollution Control, Hunan University, Ministry of Education, Changsha, 410082, China
[c] College of Physics and Microelectronics Science, Hunan University, Changsha, 410082, China

ARTICLE INFO

Article history:
Received 19 September 2015
Received in revised form
23 October 2015
Accepted 26 November 2015
Available online 2 December 2015

Keywords:
TiO_2
Branched nanorod arrays
CdS/Cu_2S heterojunction
Photoelectrochemical water splitting

ABSTRACT

This paper described a facile method for the design and utilization of three-dimensional TiO_2 branched nanorod arrays with CdS and Cu_2S quantum dots co-sensitized photoelectrode for photoelectrochemical water splitting. CdS and Cu_2S quantum dots were attached on the surface of TiO_2 BNRs by successive ionic layer adsorption and reaction (SILAR). The morphology and element composition of the fabricated samples were characterized by field emission scanning electron microscopy (FE-SEM), high resolution transmission electron microscopy (HR-TEM), energy dispersive X-ray spectroscopy (EDS), X-ray diffraction (XRD), and the optical features were measured by UV–vis diffuse reflection spectroscopy (UV–vis DRS) and photocurrent density–voltage (I–V) curves. The photocurrent value can be significantly enhanced due to the introduction of CdS and Cu_2S quantum dots on the TiO_2 BNRs surface. The 9 cycles of CdS and 6 cycles of Cu_2S presented the best performance and reached a high photocurrent density to 13.65 mA at 0 V versus Ag/AgCl and hydrogen generation efficiency of 7.74% at −0.467 V versus Ag/AgCl. This enhancement can be attributed to the improved light absorption and the heterojunction formed between CdS and Cu_2S, which can greatly promote the introduction and transportation of the photo electrons. This work provided a facile way for the synthesis of high performance photoelectrode for photoelectrochemical water splitting.

1. Introduction

Hydrogen energy, as a potential source of renewable and clean energy, has been regarded as one of the most promising candidates for traditional fossil energy. To get this kind of clean energy, numerous methods have been proposed, such as photocatalytic hydrogen production from water [1–3], photoelectrochemical (PEC) water splitting [4–6], biological hydrogen production [7,8], and etc. Recently, due to the unique properties and environmentally friendly process, PEC water splitting using semiconductor thin film as photoelectrode has attracted a lot of attention [9]. Meanwhile, many different kinds of active photocatalysts have been applied as photoelectrode materials for PEC water splitting system, such as TiO_2 [10,11], Fe_2O_3 [12,13], ZnO [14], WO_3 [15] and other complex composited semiconductors [16]. Compared with other photocatalysts, TiO_2 is currently one of the most commonly used owing to the following superior properties, good chemical stability, non-toxic and environmental friendly properties, low cost, high resistance to photocorrosion [17,18]. However, bare TiO_2 still present poor photoelectrochemcial water splitting performance, mainly due to the following reasons: (1) rapid recombination of photogenerated electrons and holes, (2) less absorption of light in the visible region [19].

So, in order to solve the first problem mentioned above, since Liu et al. had synthesized TiO_2 nanorod arrays on substrate for the first time [20], many researchers have attempted to design and synthesize a one-dimensional (1D) TiO_2 nanostructure, such as nanowire, nanorod and nanotube, in recent years [21–24].

* Corresponding author. College of Environmental Science and Engineering, Hunan University, Changsha, 410082, China.
** Corresponding author. College of Environmental Science and Engineering, Hunan University, Changsha, 410082, China.
E-mail addresses: tanglin@hnu.edu.cn (L. Tang), zgming@hnu.edu.cn (G. Zeng).

http://dx.doi.org/10.1016/j.jallcom.2015.11.206
0925-8388/

Compared with TiO_2 film comprised of nanoparticles, highly ordered TiO_2 nanorod arrays (TiO_2 NRs) offer direct electrical pathways for photogenerated electrons transfer, leading to high electron transport rates, which in turn inhibits the recombination of photogenerated electron–hole pairs [18,25]. However, the specific surface areas of bare TiO_2 nanorod arrays are usually small, which limits the light adsorption and the reaction contact area, and suppresses the performance of the TiO_2 NRs based photoelectrode in return [26]. Usually, materials with large surface area will bear high adsorption ability [27–30]. Herein, design and preparation of three-dimensional (3D) TiO_2 nanostructured photoelectrode should be a good solution to solve this problem. 3D TiO_2 nanostructured photoelectrode owns unique characteristics such as large surface areas, high carrier mobility and enhanced electron conductivity, which are beneficial to PEC water splitting [31]. Furthermore, TiO_2 branched nanorod arrays (TiO_2 BNRs) with single crystalline can increase surface area, enhance electron conductivity, and result in improved photocurrent harvest efficiencies. Wolcott et al. fabricated dense and aligned TiO_2 nanorod arrays using an oblique-angle deposition method and used the fabricated TiO_2 nanorod arrays as working electrode in photoeletrochemical water splitting system for the first time in 2009. Yang et al. have recently synthesized hierarchical TiO_2 containing both of the anatase and rutile TiO_2, and showed a photocurrent density of 2.08 mA cm^{-2} at a potential of 1.23 V versus reversible hydrogen electrode (RHE) [32]. Very recently, Liu and coworkers fabricated TiO_2 branched nanorod arrays with surface-phase junctions, which showed much better photoelectrochemical water splitting activity than the TiO_2 nanorod just with a single pure phase [33].

However, there is another non-negligible demerit that the absorption spectrum of TiO_2 photoelectrodes is limited to UV region, which only possess 4% of the whole light energy. Thus, many efforts have been made to extend the photo response region of TiO_2 to visible light. Sensitized or doped TiO_2 structure with other element or materials should be an efficient way to reach that goal, including metal (such Au [34] and Ni [35]), non-metal (such C [36], N [37] and S [38]), especially the deposition of another narrow band-gap semiconductor (such as CdS [39], CdSe [40], $ZnIn_2S_4$ [41]). TiO_2 incorporated with sulfide semiconductors has been proved to be a very effective way to narrow its band gap and enhance its hydrogen production efficiency [42]. Su et al. fabricated CdS quantum dots (QDs) sensitized TiO_2 branched nanorod arrays by a hydrothermal method, which performed a remarkable photocurrent density to ~4 mA cm^{-2} at 0 V versus Ag/AgCl [26]. Guo and co-workers had achieved a high density of 24.85 mA cm^{-2} at 0.92 V versus Ag/AgCl and a much higher hydrogen generation efficiency of 13.15% at 0.70 V versus Ag/AgCl, which was ascribed to the effect of the Cu_2S composite coated on the surface of TiO_2 branched nanorod arrays [19]. According the results mentioned above, the high performance of the CdS or Cu_2S doped TiO_2 nanorod arrays can be attributed to the heterostructure formed between the CdS and TiO_2 or the Cu_2S and TiO_2. Due to the existence of narrow-wide band semiconductors, more visible light can be absorbed and utilized in the complex system. And the existence of the formed heterostructure can facilitates the transport of electrons and hinders the recombination of photosensitized electrons and holes. To further improve the performance, two narrow semiconductors co-doped TiO_2 has also been studied [43,44]. Li and coworkers had synthesized CdS and CdSe co-doped TiO_2 nanowire arrays and presented high performance than CdS or CdSe doped TiO_2 for solar cell application [44]. These results indicated that two narrow semiconductors co-doped TiO_2 would be more efficient for solar energy utilization than single semiconductor doped one. Herein, TiO_2 BNRs co-sensitized with CdS and Cu_2S to form heterostructure on the surface of the TiO_2 BNRs should be an efficient way to fabricate TiO_2 BNRs based photoelectrodes with extended absorption in the visible region and high PEC activity. CdS is a good sensitized material, and Cu_2S is highlighted because of its non-toxic, low cost and earth-abundant properties. The band-gap of bulk Cu_2S is 1.20 eV, which can make Cu_2S become a widely used photosensitizer for various wide band-gap semiconductor photoanodes [19,45], solar energy devices [46,47], and photocatalytic degradation of environment containments [48]. Although the composite based on CdS and Cu_2S had been studied in different areas and presented great performance [49], to the best of our knowledge, the synthesis of CdS and Cu_2S co-sensitized to TiO_2 BNRs nanostructures for PEC water splitting system and how the formed nanoscale heterojunction promote the light utilization and charge separation have seldom been investigated.

Herein, we successfully synthesized high densities of rutile TiO_2 BNRs with enhanced surface-to-volume ratios on fluorine-doped tin oxide (FTO) substrate by combining a facile hydrothermal and a chemical method. Then CdS QDs and Cu_2S QDs were decorated onto the surface of the TiO_2 BNRs by successive ionic layer absorption and reaction (SILAR). To illustrate the effect of the nanostructure and heterostructure, two major kinds of PEC electrodes, TiO_2 BNRs/CdS PEC electrode and TiO_2 BNRs/CdS/Cu_2S PEC electrode were designed and synthesized. The performances of the two PEC electrodes in water splitting system were compared, including photocurrent density and photoconversion. The good performance of the TiO_2 BNRs/CdS/Cu_2S electrode indicated its potential application in PEC water splitting. Furthermore, the detailed working mechanism of the composite was also discussed.

2. Experimental

2.1. Materials

Titanium tetrachloride ($TiCl_4$, ≥99.9%) and titanium butoxide (TBOT, ≥99%) were purchased from Aladdin Industrial Corporation, Fluorine-doped tin oxide (FTO) glass were purchased from Zhuhai Kaivo Optoelectronic Technology Co., Ltd. Concentrated hydrochloric acid (HCl), acetone, 2-propanol and ethanol were purchased from Sinopharm Chemical Reagent Co., Ltd. (China). All reagents and solvents were of analytical reagent grade and used without further purification. Deionized water (18.25 MΩ cm) from a Millipore Q water purification system was used in all experiments.

2.2. Preparation of TiO_2 seeded layer on the FTO substrate

Prior to the deposition of TiO_2 seeds, the FTO substrate (F: SnO_2, 15 Ω) was ultrasonically cleaned in a mixed solution of deionized water, acetone and 2-propanol (volume rations of 1:1:1) for 60 min, then dried under N_2 flow. The TiO_2 seeded layer was prepared by soaking the washed FTO substrate into 0.15 M $TiCl_4$ aqueous solution and hold at 70 °C for 30 min, followed by rinsing with deionized water and ethanol, and then annealed at 450 °C for 30 min.

2.3. Preparation of TiO_2 nanorod arrays

The TiO_2 nanorod array (TiO_2 NRs) was prepared using a hydrothermal method reported previously with some modification [20]. Typically, 25 ml of deionized water and 25 ml of concentrated hydrochloric acid (mass fraction 36.5–38%) were mixed and stirred for 10 min, and then 0.8 ml of titanium butoxide was added dropwise into the mixed solution. The mixture was stirred for another 10 min to make sure that the solution was transparent. The mixture was then transferred to a 100 ml volume of Teflon-lined stainless steel autoclave, where a seeded FTO substrate

(4 cm × 2 cm) was placed at an angle against the wall of the Teflon-lined with the conducting side facing down. Then the sealed autoclave was kept at 170 °C for 6 h and cooled down to room temperature naturally. When the reaction was finished, the obtained product was rinsed thoroughly with ethanol and deionized water for several times and dried in an oven at 60 °C.

2.4. Preparation of branched TiO_2 nanorods

The TiO_2 branched nanorod arrays were obtained via a simple aqueous chemical growth method. First of all, the prepared TiO_2 NRs sample was immersed in a 0.2 M $TiCl_4$ aqueous solution at 25 °C for 18 h. Secondly, the TiO_2 BNRs were taken out and rinsed with pure ethanol. Finally, the sample was dried at 60 °C and annealed at 450 °C for 30 min.

2.5. Preparation of CdS QDs sensitized TiO_2 branched nanorod arrays

CdS QDs were deposited onto the TiO_2 BNRs by successive ion layer absorption and reaction technique (SILAR). Briefly, the prepared TiO_2 BNRs was dipped into a 0.1 M $Cd(NO_3)_2$ aqueous solution for 5 min, followed by immersing in deionized water for 60 s. And then the TiO_2 BNRs with Cd^{2+} were dipped into a 0.1 M Na_2S aqueous solution for 5 min followed by immersing in deionized water for 60 s. Therefore, one cycle of CdS deposition on the TiO_2 BNRs has been completed, and several cycles were conducted to obtain the desired deposition of CdS QDs. The following chemical reactions could take place during the SILAR cycle:

$$Cd^{2+} + S^{2+} \rightarrow CdS$$

2.6. Preparation of CdS and Cu_2S QDs co-sensitized TiO_2 branched nanorod arrays

The preparation of TiO_2 BNRs/CdS/Cu_2S was conducted in the base of optimal TiO_2 BNRs/CdS. In this process, the saturated CuCl aqueous and 5 mM Na_2S were used to deposit Cu_2S nanoparticles on TiO_2 BNRs/CdS samples to obtain the TiO_2 BNRs/CdS/Cu_2S photoelectrochemical (PEC) electrodes. Typically, the TiO_2 BNRs/CdS sample was firstly immersed in the saturated CuCl aqueous solution for 60 s, and then immersed in a large amount of deionized water for 60 s. Subsequently, the sample with Cu^+ was immersed in the Na_2S aqueous solution for 60 s. Finally, the sample was immersed in deionized water for 60 s. The above SILAR process was one cycle of Cu_2S deposition of TiO_2 BNRs/CdS. The desired amount of Cu_2S can be achieved by repeating the assembly cycles. The following chemical reactions could take place during the SILAR cycle:

$$2Cu^{+} + S^{2-} \rightarrow Cu_2S$$

2.7. Materials characterization

Field-emission scanning electron microscopy (FE-SEM) (Hitachi S-4800, Japan) was used to study the morphology of the samples at an accelerating voltage of 5 kV. More detailed structural examinations were carried out by transmission electron microscopy (TEM, Tecnai G2 F20 S-TWIN) and high-resolution TEM (HR-TEM) at an accelerating voltage of 200 KV. Prior to the TEM and HRTEM measurements, the branched nanorod arrays were detached from the FTO substrate and ultrasonically dispersed in ethanol, and scattered on a micro grid with a lacey carbon. The ultraviolet visible diffuse reflectance spectra (DRS) of the prepared TiO_2 NRs, TiO_2 BNRs, TiO_2 BNRs/CdS, and TiO_2 BNRs/CdS/Cu_2S in different SILAR cycles were performed on a UV–Vis spectrophotometer (Cary 300,

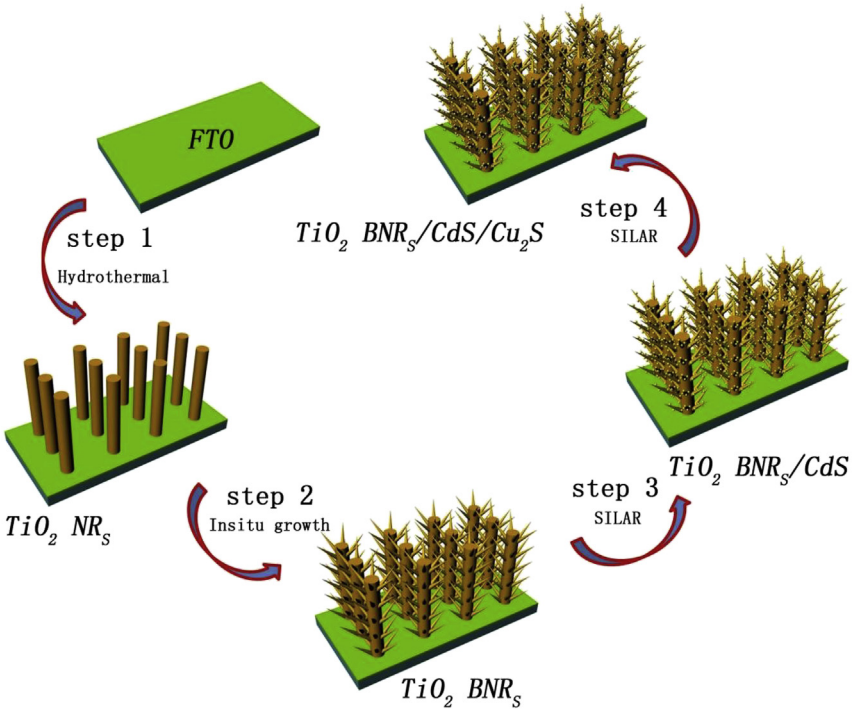

Fig. 1. Schematic illustration for the synthesis route of the TiO_2 BNRs/CdS/Cu_2S.

USA) with an integrating sphere. The crystal structure of the sample was investigated using an X-ray diffractometer (Bruker D8 Advance), and the XRD patterns of the samples were measured directly on the FTO substrate.

2.8. Photoelectrochemical characterization and measurements

Photocurrent measurements of the TiO_2 NRs, TiO_2 BNRs, TiO_2 BNRs/CdS and TiO_2 BNRs/CdS/Cu_2S electrodes were performed using a three-electrode configuration, with the nanostructure

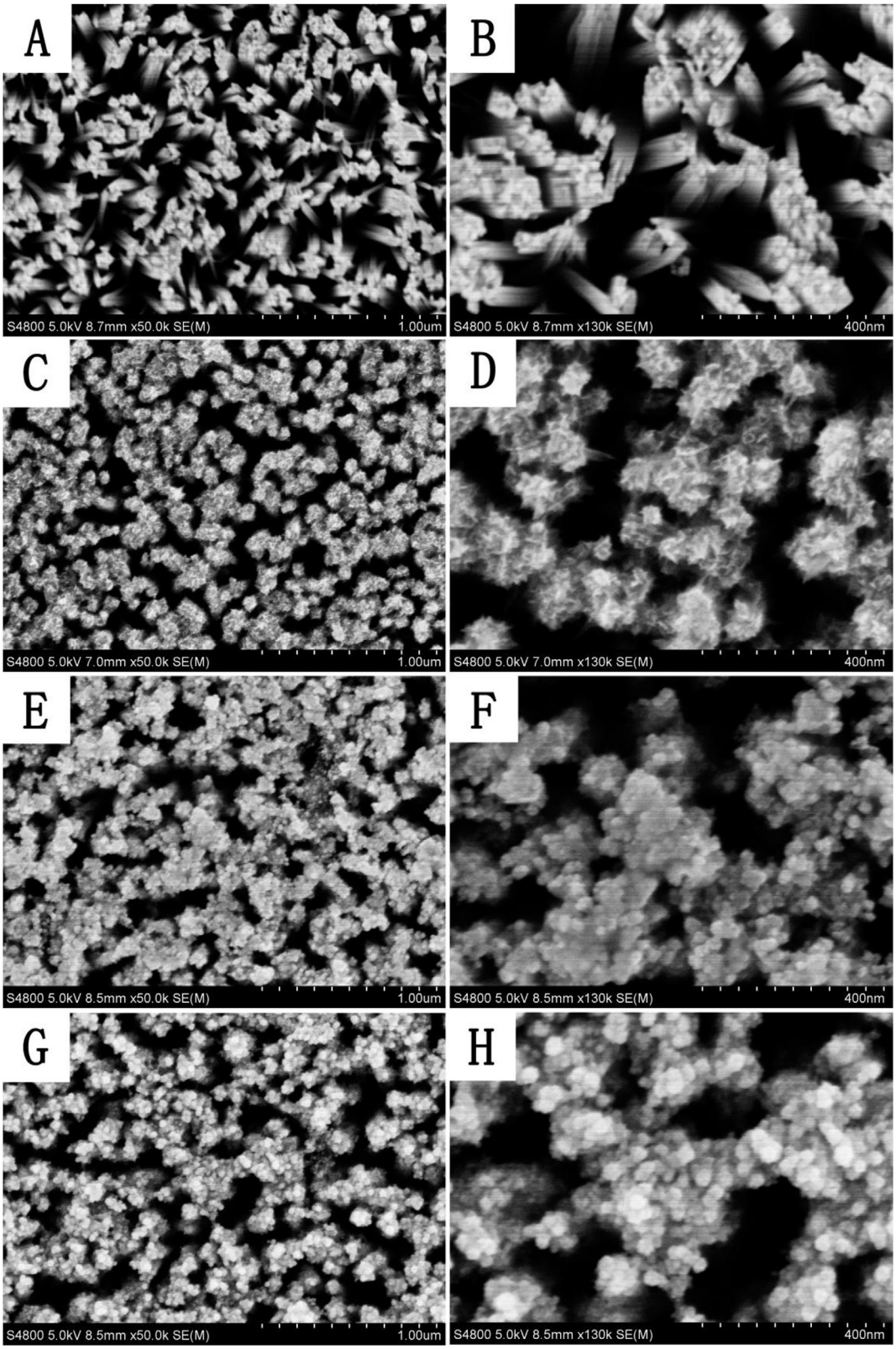

Fig. 2. FESEM images of the top view of the as prepared samples: (A and B) TiO_2 NRs, (C and D) TiO_2 BNRs, (E and F) TiO_2 BNRs/CdS (9), (G and H) TiO_2 BNRs/CdS(9)/Cu_2S (6).

materials (TiO_2 NRs, TiO_2 BNRs, TiO_2 BNRs/CdS or TiO_2 BNRs/CdS/Cu_2S) on FTO as the working electrode, saturated Ag/AgCl and platinum electrode as the counter electrode and the reference electrode, respectively. A mixed aqueous solution containing 0.35 M Na_2S and 0.25 M Na_2SO_3 was used as the electrolyte. A CHI 660D electrochemical workstation was used for linear sweep voltammetry (I–V) measurement with a scan rate of 50 mV s^{-1} and amperometry (I–t) measurement. The study of I–t measurement was conducted at a potential of 0 V versus Ag/AgCl. The illuminated area of the working electrode was about 1 cm^2. A 300 W xenon lamp (Beijing Perfectlight Technology Co. Lt, PLS-SXE 300C) was used as the light source throughout all the tests, the power intensity of the light was 100 mW cm^{-2}.

3. Result and discussion

3.1. Structure characteristics

As shown in Fig. 1, the synthesis of the TiO_2 BNRs/CdS/Cu_2S is a four-step solution-based process, which comprises the growth of the TiO_2 NRs, the assemble of the branches onto the surface of the TiO_2 NRs to form the TiO_2 BNRs by an aqueous chemical method, and the formation of the TiO_2 BNRs/CdS/Cu_2S by two successive ion layer absorption and reaction technique (SILAR) process. For the detailed preparation process, in the first step, TiO_2 crystal nucleus were formed on the FTO substrate in advance by immersing the FTO in the $TiCl_4$ aqueous solution after annealing in air, then 6 M concentrated hydrochloric acid was used to control the hydrolysis rate of the titanium butoxide, which could keep the growth of the nanorod slowly and stably. As the time went on, TiO_2 nanorod arrays began to grow on the FTO substrate. And nearly all of the TiO_2 NRs was perpendicular due to the preformed TiO_2 nucleus on the FTO substrate. Step 2 was the growth of the branches onto the surface of the TiO_2 NRs using a simple chemical growth method by immersing the TiO_2 NRs into low concentration of $TiCl_4$ aqueous solution. In step 3, TiO_2 BNRs/CdS composite structure was prepared by SILAR method. $Cd(NO_3)_2$ and Na_2S were used to deposit CdS QDs on TiO_2 BNRs for obtaining the PEC electrode. The

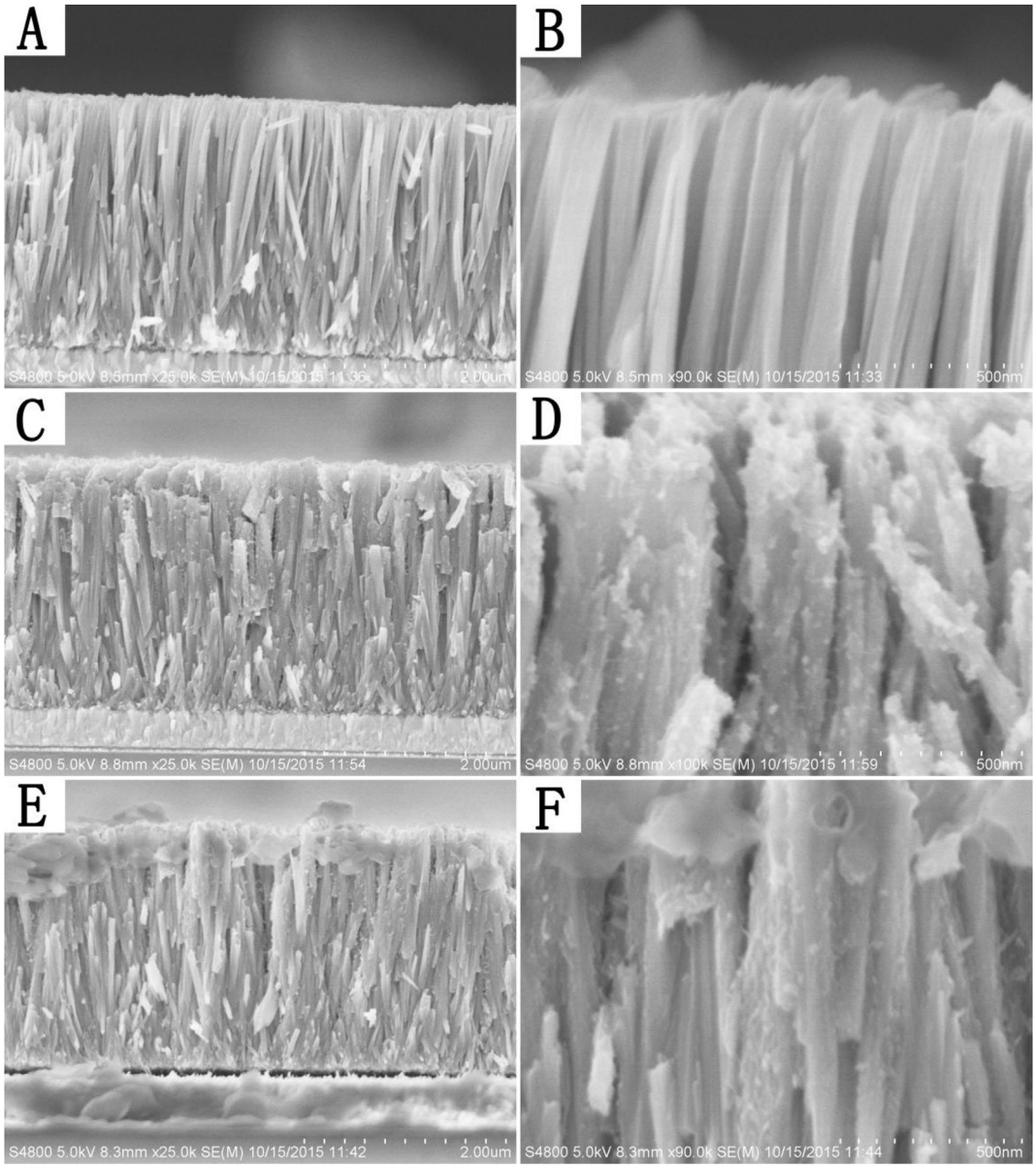

Fig. 3. FESEM images of the cross-sectional view of the as prepared samples: (A and B) TiO_2 NRs, (C and D) TiO_2 BNRs, (E and F) TiO_2 BNRs/CdS(9)/Cu_2S(6).

formation of the TiO_2 BNRs/CdS/Cu_2S in step 4 was similar to the step 3, also using the SILAR method. But the cationic precursor solution and anionic precursor solution were replaced by saturated CuCl and different concentration of Na_2S, and the immersing time was also changed.

The typical field-emission scanning microscopy (FESEM) images and the cross-section view of the samples are shown in Fig. 2 and Fig. 3, respectively. As seen in Fig. 2A and B, the TiO_2 NRs grew directly on the FTO substrate with an average diameter of ~50 nm. Besides, the TiO_2 NRs have grown vertically in the FTO substrate, and the surface of the TiO_2 NRs is smooth, with the length of about 2.2 μm (Fig. 3A and B). After the chemical treatment of TiO_2 NRs with $TiCl_4$ aqueous solution, TiO_2 BNRs were obtained as shown in Fig. 2C and D. The TiO_2 NRs was assembled with secondary nanostructure regularly and showed a branched characteristic, and each TiO_2 NRs was attached by TiO_2 branched, which improved the surface area and the roughness factor of the original TiO_2 NRs greatly (Fig. 3C and D). Just as shown in Fig. 2E and F, there are many nanoparticles on the TiO_2 BNRs after being sensitized with CdS for nine SILAR cycles, which means that the CdS QDs were successfully decorated on the TiO_2 BNRs. And as shown in Fig. 2G and H, there are more nanoparticles on the TiO_2 BNRs due to the Cu_2S formed followed by six SILAR cycles on the surface of the TiO_2 BNRs/CdS(9), these changes also can be found in Fig. 3E and F. It indicates that the CdS and Cu_2S QDs were coated over the branches uniformly, which is critical to obtaining good photoelectrochemical properties. In order to further determine the existence of CdS and Cu_2S in TiO_2 BNRs/CdS/Cu_2S, energy dispersive X-ray spectroscopy (EDS) and SEM elemental mapping were employed. As shown in Fig. 4 and Fig. S1, atomic ratio of the Cu, Cd and S is 0.82:0.52:1.20, and the Cu, Cd and S elements are present uniformly in the synthesized samples. These results further demonstrate the successfully coating of CdS and Cu_2S QDs on the TiO_2 BNRs. The EDS data of original TiO_2 BNRs and TiO_2 BNRs/CdS are also shown in Fig. S2 for comparison. Besides, the detailed microscopic morphology of the TiO_2 BNRs and TiO_2 BNRs/CdS/Cu_2S nanostructure was characterized using transmission electron microscopy (TEM), high-resolution TEM (HR-TEM) and selected area electron diffraction (SAED). It can be seen that in the TEM image of the TiO_2 BNRs in Fig. 5A, the branches grew along the backbone of the TiO_2 NRs, which means a 3D nanostructure has

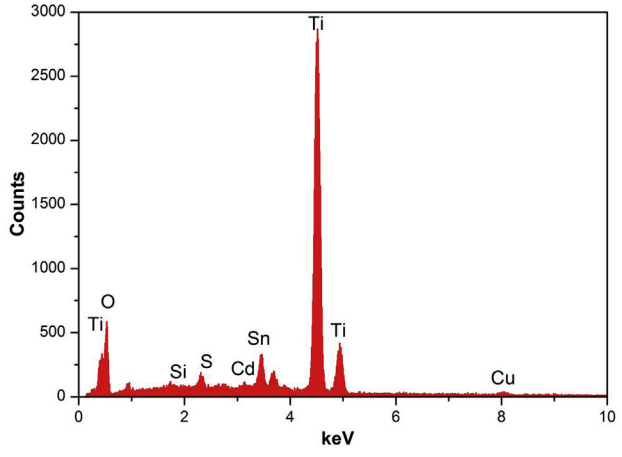

Element	O-K	Si-K	S-K	Cd-L	Sn-L	Ti-K	Cu-K
Weight %	30.36	00.62	01.25	01.90	09.09	55.10	01.68
Atom %	58.77	00.69	01.20	00.52	02.37	35.63	00.82

Fig. 4. EDS patterns of the TiO_2 BNRs/CdS(9)/Cu_2S(6) composite structure.

been prepared in this study. The corresponding HRTEM images of the TiO_2 BNRs are shown in Fig. 5B. It can be seen that the distance between the adjacent lattice fringes is 0.229 nm, which can be exactly matched to the interplanar distance of the (200) crystalline plane of rutile TiO_2 (JCPDS No. 21-1276). The relative selected area electron diffraction (SAED) of the TiO_2 BNRs was shown in Fig. 5C, the well-aligned spots present the single crystalline of the TiO_2 BNRs. Fig. 5D is a typical TEM image of the TiO_2 BNRs/CdS/Cu_2S, which shows clearly that the surface of the TiO_2 branched nanorod arrays is covered by CdS/Cu_2S, and even further confirms that CdS/Cu_2S have been deposited on TiO_2 BNRs successfully. HR-TEM image of the TiO_2 BNRs/CdS/Cu_2S is shown in Fig. 5E. The adjacent lattice spacing measured for the crystalline plane is 0.324 nm, which corresponds to the (110) plane of rutile TiO_2. By carefully measuring the lattice parameters and referring to the data in JCPDS card, the lattice spacing of the crystallites close to TiO_2 is 0.336 nm, which can be attributed to the (002) plane of CdS (JCPDS No. 65-3414), and the lattice fringe of the outer crystalline connects to the CdS layer is of 0.198 nm, which is in agreement with the (110) plane of Cu_2S (JCPDS No. 26-1116). From the relative apparent spot diffraction patterns shown in Fig. 5F, it can be clearly observed that the bright spots come from single crystalline TiO_2, and the diffraction rings originate from the polycrystalline CdS and Cu_2S, which could further confirm that Cu_2S and CdS have been deposited in the TiO_2 BNRs successfully [50,51].

XRD patterns of the fabricated samples are shown in Fig. 6. The peaks of the SnO_2 are corresponding to the tetragonal rutile phase (JCPDS No. 41-1445). All the diffraction peaks of TiO_2 agree well with the tetragonal rutile phase (JCPDS No. 21-1276). The significantly enhanced (002) peaks indicates that the nanorod arrays are well crystalized and grown perpendicularly to the FTO substrate along the [001] direction, and the absence of other peaks means that the whole TiO_2 BNRs are single crystal of rutile. When the CdS QDs were introduced on TiO_2 BNRs surface, a small peak can be found in the XRD pattern of TiO_2 BNRs/CdS, which belongs to (110) of CdS (JCPDS No. 65-3414). But we also note that no Cu_2S peaks can be observed in TiO_2 BNRs/CdS/Cu_2S, which is probably due to the fact that the Cu_2S QDs were mostly covered and dispersed on the surface TiO_2 BNRs, and the mass fraction of the loaded Cu_2S QDs is very low. All these results above provide strong evidence for the successful coating of CdS and Cu_2S QDs on the surface of TiO_2 BNRs and the formation of TiO_2 BNRs/CdS/Cu_2S cascade structure.

3.2. Optical properties

Fig. 7 displays the light absorption range of TiO_2 NRs, TiO_2 BNRs, TiO_2 BNRs/CdS, and TiO_2 BNRs/CdS/Cu_2S. It is clear to see that TiO_2 NRs mainly absorb UV light with a wavelength below 420 nm, which can be attributed to their relative large band gap (rutile TiO_2, ~3.0 eV). However, upon the surface of the TiO_2 NRs were assembled with TiO_2 branches, more light can be absorbed, and the rate of the light reflection could also be increased between the TiO_2 branches on TiO_2 BNRs, which presents great advantages over original TiO_2 NRs. But once the CdS QDs were sensitized upon the TiO_2 BNRs for 9 cycles, the absorption range of the composite could be extended to ~550 nm, showing an effective absorption property in the visible light. Especially, when the coating of Cu_2S QDs were assembled by 6 SILAR cycles deposition, the adsorption properties of the synthesized sample (TiO_2 BNRs/CdS/Cu_2S) were further increased in the visible region. This phenomenon can be explained mainly by the reason that the TiO_2 BNRs/CdS/Cu_2S can make better use of the sunlight. First of all, light would be able to be reflected much more times among the branches, and the existence of the CdS and Cu_2S QDs can also enhance that process and extend the light transmission path, which will eventually be beneficial to the full

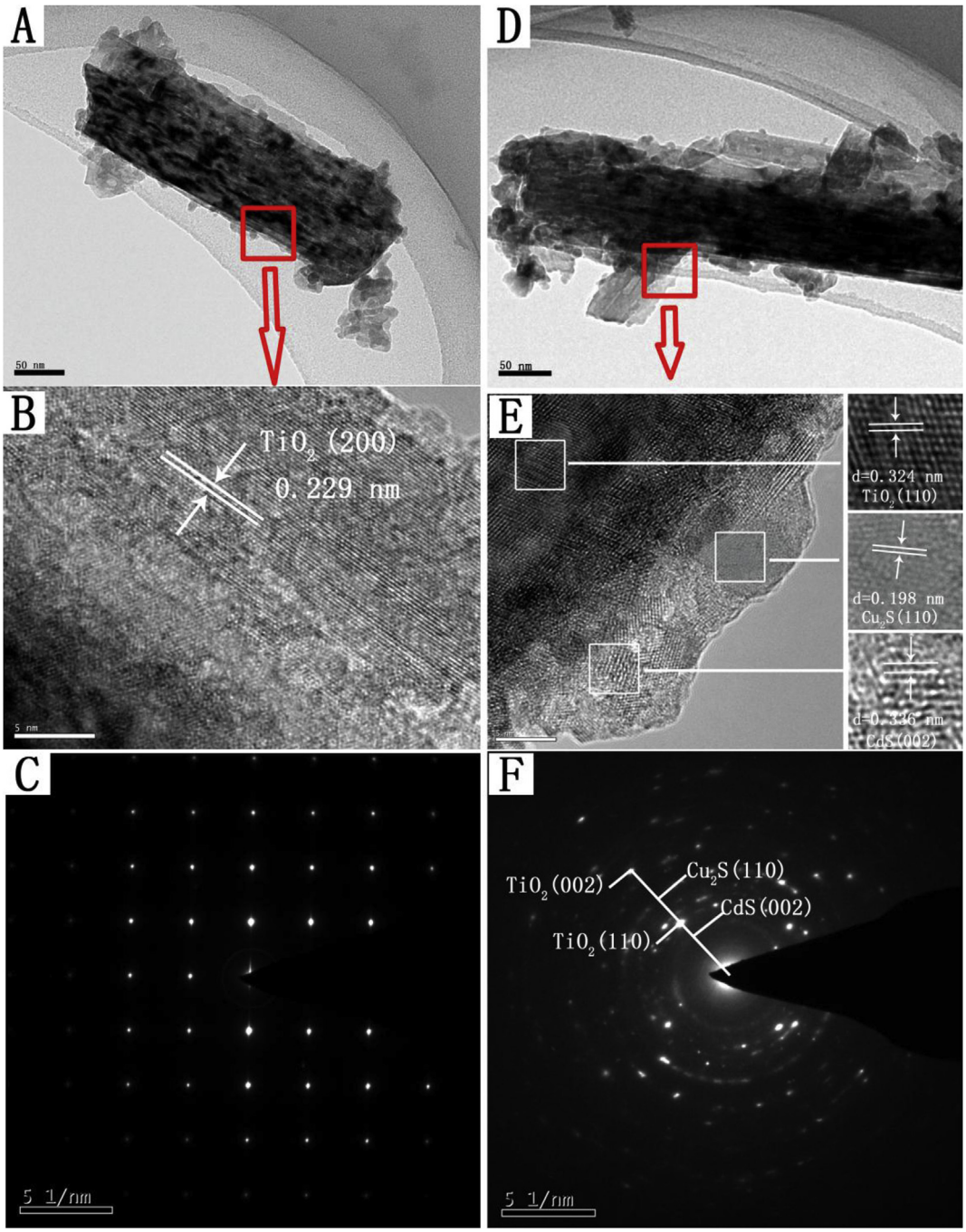

Fig. 5. TEM image (A), HR-TEM image (B) and SAED image (C) of TiO_2 BNRs. TEM image (D) and HR-TEM image (E) and SAED image (F) of the TiO_2 BNRs/CdS/Cu_2S.

utilization of the incident sunlight. And meanwhile, for the TiO_2 BNRs/CdS/Cu_2S composite structure, a high efficiency of light harvesting can be obtained by fabricating well-aligned TiO_2 BNRs as photoelectrode. The synergistic reaction between CdS and Cu_2S on the surface of the TiO_2 BNRs can improve the light utilization efficiency by reflecting unabsorbed photons back to the TiO_2 BNRs, which can greatly improve the utilization efficiency of the incident light. Besides, due to the high surface areas obtained for the branches attached on the surface of the TiO_2 BNRs, a layer of accumulated CdS and Cu_2S QDs can trap relatively more photons, and herein, large amount of protons can be utilized by the TiO_2 BNRs/CdS/Cu_2S composite for producing photosensitized electron/hole pairs. What's more, the perpendicular growth of the TiO_2 nanorod arrays can provide a high speed transport routes for the photo-sensitized electrons transfer, which takes full advantages of the excellent carrier transport performance of the as-obtained materials. Owing to the narrow band-gap of CdS and Cu_2S, and the synergistic function between the two nanoparticles, the TiO_2 BNRs/CdS/Cu_2S can absorb more visible light, which provides a more extensive range of adsorption spectrum than bare TiO_2 BNRs and CdS QDs coated TiO_2 BNRs.

3.3. Photoelectrochemical characteristics

The PEC properties of the prepared various composite structures were studied by relying on a three-electrode PEC system. Fig. 8A

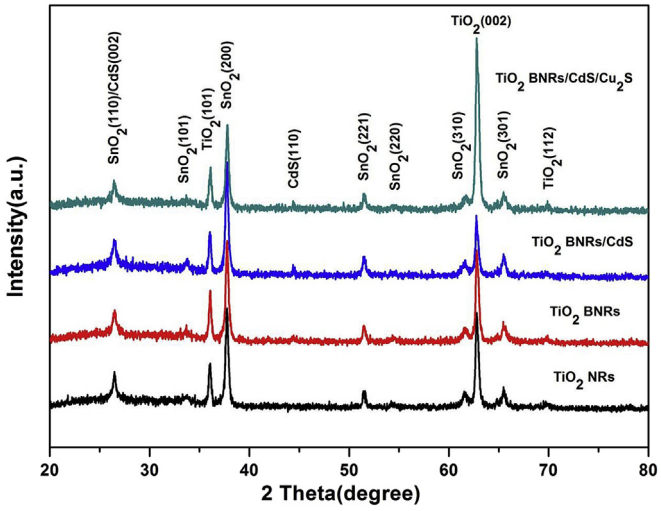

Fig. 6. XRD patterns of TiO_2 NRs, TiO_2 BNRs, TiO_2 BNRs/CdS and TiO_2 BNRs/CdS/Cu_2S.

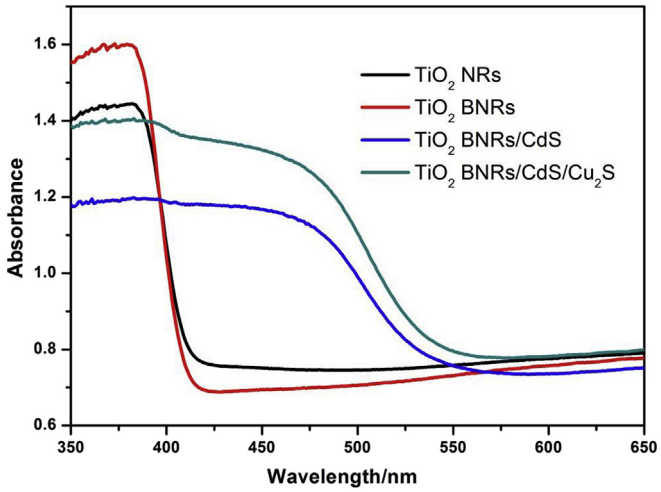

Fig. 7. UV–Vis diffuse reflectance spectra of TiO_2 NRs, TiO_2 BNRs, TiO_2 BNRs/CdS(9) and TiO_2 BNRs/CdS(9)/Cu_2S(6).

displays the photocurrent density–voltage characteristics of TiO_2 NRs, TiO_2 BNRs and different SILAR cycles of CdS QDs sensitized TiO_2 BNRs. It can be found that the photocurrent densities of the TiO_2 NRs was the lowest, while after the branches growing around the backbone of the TiO_2 Nanorod arrays to form the TiO_2 branched nanorod arrays, the photocurrent density was increased. And meanwhile, once the CdS QDs was coated on the surface of the TiO_2 BNRs, the current density was increased again and gradually promoted with the increase of the CdS QDs cycles at initial stage (from 1 cycle to 9 cycles). However, when further increasing the SILAR cycles of CdS QDs (from 9 cycles to 11 cycles), the photocurrent density was reduced. The variation trend of photocurrent density (at 0 V versus Ag/AgCl) as a function of CdS QDs cycles are shown in Fig. 8B. It can be observed that 9 cycles of deposition of CdS QDs on TiO_2 BNRs make the photoelectrochemical system exhibit the best

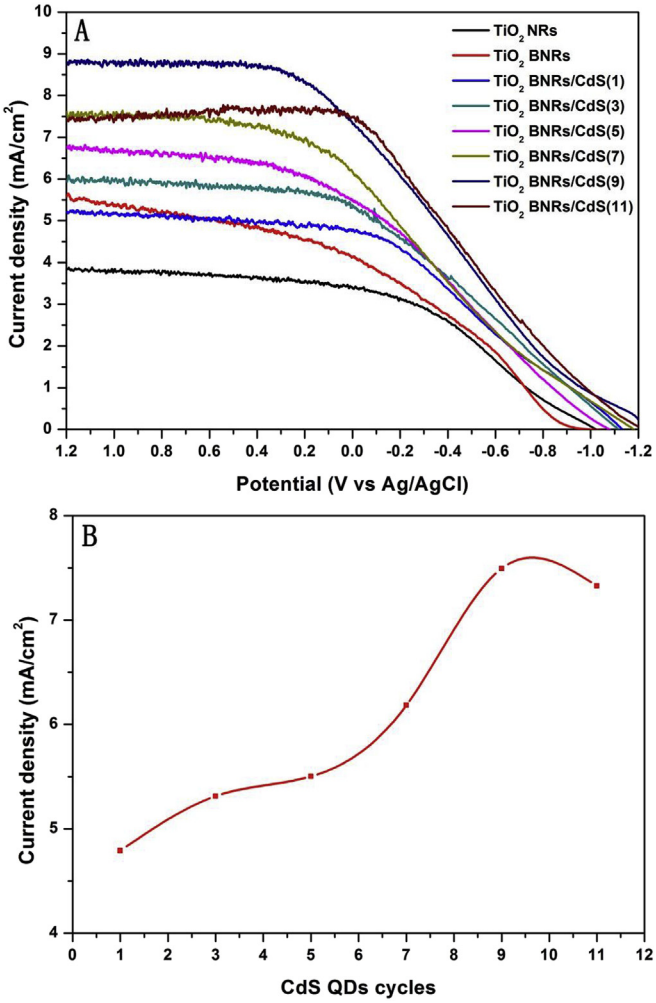

Fig. 8. (A)Photocurrent density–voltage characteristics of TiO_2 NRs, TiO_2 BNRs and different SILAR cycle of CdS QDs sensitized TiO_2; (B) Variation of the current density as a function of SILAR cycles of CdS QDs.

photovoltaic performance. Based on the optimal cycle number of CdS QDs, different SILAR cycles of Cu_2S decorated TiO_2 BNRs/CdS(9) are investigated to seek the influence of the Cu_2S layers on the performance of the CdS/Cu_2S co-sensitized photoelectrode for photoelectrochemical water splitting. Fig. 9A shows the variation of I–V curves with the increase of Cu_2S QDs SILAR cycles on TiO_2 BNRs/CdS(9) electrode based PEC system. Significant improvement of photocurrent density is observed with the Cu_2S cycle increasing from 2 to 6. Appropriate increase of SILAR cycles can enlarge the loading amount Cu_2S QDs, which in turn results in more light absorption to generate photoexcited electrons, while the photocurrent density (at 0 V versus Ag/AgCl) decreased when the excessive SILAR cycles (from 6 cycles to 10 cycles) was added to the surface of TiO_2 BNRs (Fig. 9B).

The corresponding light energy of different samples to chemical energy conversion (photoconversion) efficiency is shown in Fig. 9C. Photoconversion efficiency of η is calculated as follows [5,52,53]:

$$\eta = [(\text{total power output} - \text{electrical power input})/\text{light power input}] \times 100$$
$$= j_p\left[E^0_{rev} - \left|E_{app}\right|/I_0\right] \times 100$$

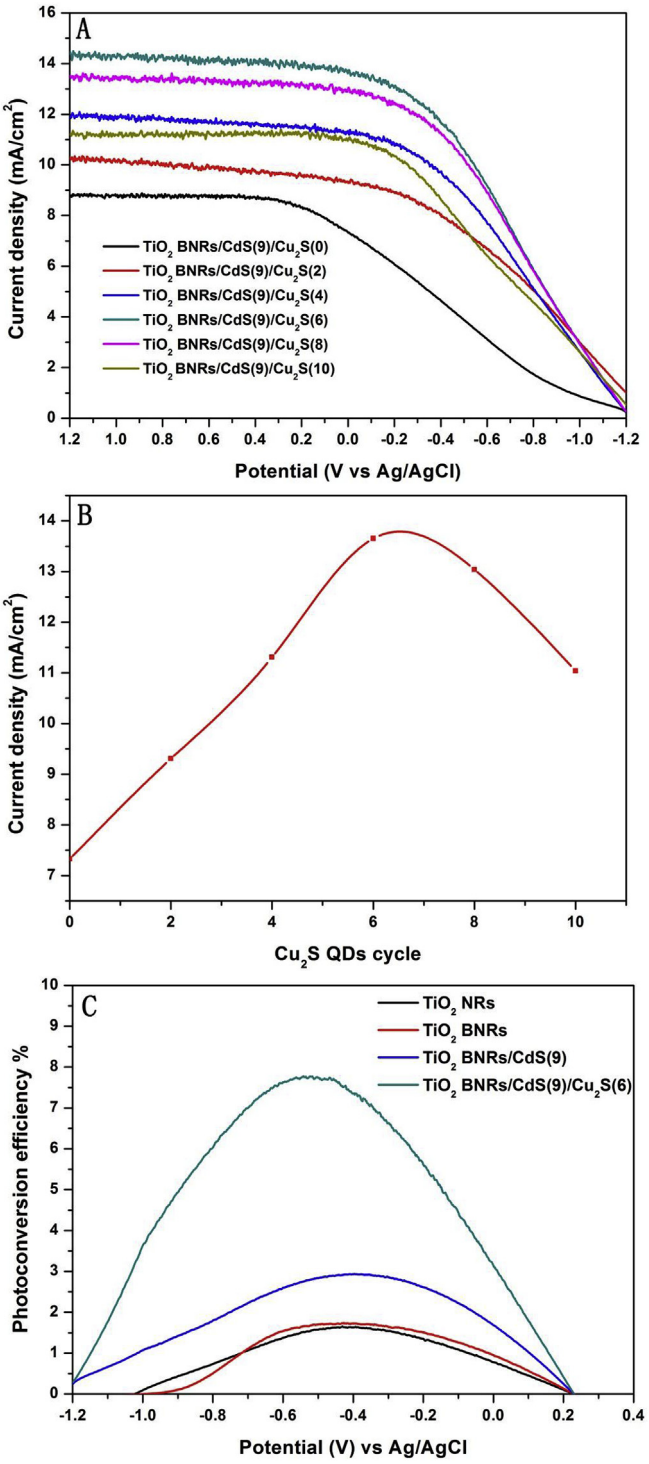

Fig. 9. (A)Photocurrent density–voltage characteristics of different SIRAR cycles of Cu_2S QDs on TiO_2 BNRs/CdS (9); (B) Variation of the current density as a function of SILAR cycle of Cu_2S QDs; (C)Photoconversion efficiencies of TiO_2 NRs, TiO_2 BNRs, TiO_2 BNRs/CdS (9) and TiO_2 BNRs/CdS (9)/Cu_2S (6) samples calculated from the line weep voltammograms.

$$E_{app} = E_{meas} - E_{aoc}$$

where j_p is the photocurrent density (mA cm^{-2}); I_0 is the power density of incident light (mW cm^{-2}); E^0_{rev} is 1.23 V/NHE; E_{app} is the applied potential (vs Ag/AgCl); E_{meas} is the potential (vs Ag/AgCl) of the working electrode potential at which photocurrent was measured under illumination; and E_{aoc} is the electrode potential (vs Ag/AgCl) of the same working electrode at open circuit conditions in the same electrolyte and under the same illumination. From Fig. 9C, it can been seen that the different highest efficiencies of ca. 1.65%, 1.73%, 2.94% and 7.74% are obtained for TiO_2 NRs, TiO_2 BNRs, TiO_2 BNRs/CdS(9) and TiO_2 BNRs/CdS(9)/Cu_2S(6) electrodes, respectively.

The different activity of the TiO_2 NRs, TiO_2 BNRs, TiO_2 BNRs/CdS and TiO_2 BNRs/CdS/Cu_2S can be explained using schematic diagrams as shown in Fig. 10. In Fig. 10A, the surface of the TiO_2 nanorod arrays was smooth, which limits the light reflection among the TiO_2 nanorod arrays. But when the branches was grown around the backbone of the nanorod, there is more light reflection among the branched nanorod arrays, which indicates the increasing use of the incident light (Fig. 10B). As shown in Fig. 10C, when the CdS QDs was coated on the surface of the TiO_2 BNRs, the TiO_2 BNRs/CdS can not only absorb UV light and keep more reflection due to the existence of the branches, but the visible light can also be utilized owing to the presence of CdS QDs. Because of the narrow band gap (2.25 eV), CdS QDs can broaden the upper light response limit from ~420 nm to ~550 nm, which will greatly increase the production of photosensitized electron/hole pairs. However, when excessive CdS QDs were coated, and the CdS SILAR was conducted more than 9 cycles, the aggregates of CdS QDs can occur at the surface of the TiO_2 BNRs, which leads to larger particle size of CdS. These large CdS particles will cause the disappearance of the quantum effect and are not conductive to the multiple electrons generation from the adsorption and sensitization of a single photon. What's more, the aggregated CdS crystallites will increase the recombination ratio of the photoelectrons and holes, which will lead to the decrease of the photoelectrochemical performance. The result that the photoelectrochemical activity depends on the amount of photoactive compounds is similar to the reported studies [54,55]. In Fig. 10D, the Cu_2S QDs were coated based on the optimal TiO_2 BNRs/CdS, the photocurrent density can further increase with the decoration of Cu_2S QDs on the surface of the TiO_2 BNRs/CdS(9), which can be explained by the following two aspect. On one hand, due to the relative narrow band gap of Cu_2S (1.20 eV), Cu_2S can increase the utilization efficiency of the incident light, and result in the more efficient charge separation in CdS QDs, which can further improve the transportation of the photosensitized electron and reduce the recombination of the photosentized electrons and holes, so the performance of the whole PEC system will be promoted in turn. On the other hand, just as shown in Fig. 11, as we know, the band gap of TiO_2, CdS and Cu_2S are 3.2 eV, 2.25 eV and 1.20 eV, respectively. When they are in bulk, their band-gap cannot match well to provide a good path for the transportation of the electrons due to that the conductor band of Cu_2S is lower than that of CdS, which will inhibit the photosensitized electrons transport from the Cu_2S to CdS. But just as mentioned above, when Cu_2S nanoparticles were coated on the CdS QDs, a great number of nanoscale heterostructure could be produced between the two semiconductors. Considering the band structures of the Cu_2S and CdS, it has been reported by other groups that both of the valance band (VB) and the conduction band (CB) of CdS are lower than those of Cu_2S [49,56]. When the heterojunction formed between TiO_2 and CdS, and the heterostructure formed between Cu_2S and CdS, the electron transfer occurred from Cu_2S to CdS, and eventually to TiO_2. While the hole transfer occurred from TiO_2 to CdS and then from CdS to Cu_2S due to the different Fermi levels alignment when the system reached equilibration state. And when the Cu_2S SILAR reached 6 cycles, the interaction between Cu_2S and CdS achieved the best effect. However, when the SILAR cycles continued to increase, the surface of CdS QDs was nearly covered by

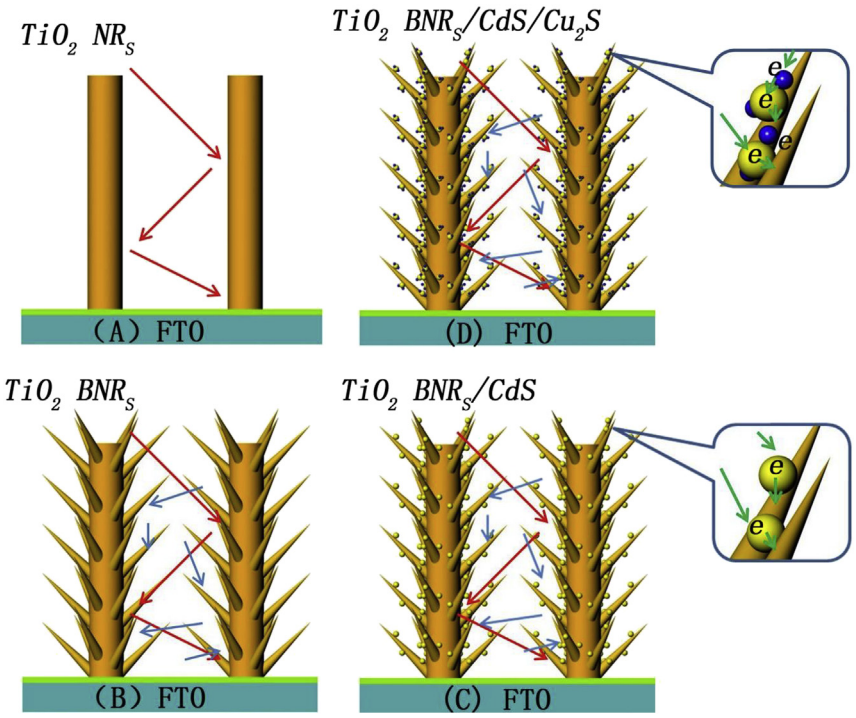

Fig. 10. Schematic representation of the incident sunlight utilization in TiO_2 NRs, TiO_2 BNRs, TiO_2 BNRs/CdS and TiO_2 BNRs/CdS/Cu_2S.

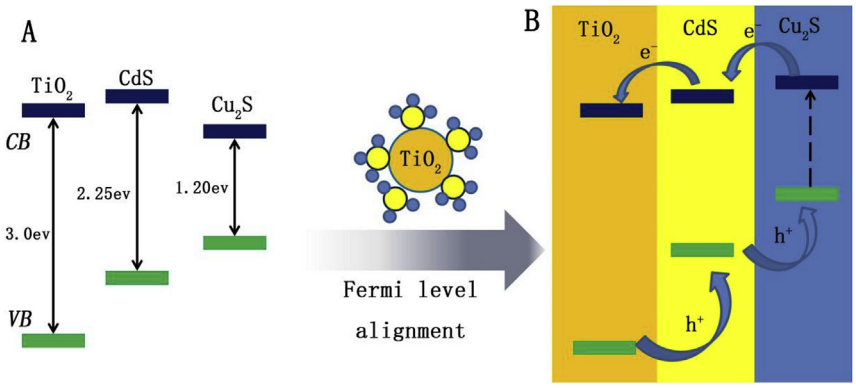

Fig. 11. (A) Relative band position of TiO_2, CdS and Cu_2S in bulk and (B) ideal stepwise structure of band edges for the efficient transport of the excited electrons and holes in TiO_2/CdS/Cu_2S photoelectrode.

Cu_2S nanoparticles, which would reduce the formation of more heterostructure and affect the efficient utilization of light by CdS nanoparticles. Meanwhile, more Cu_2S nanoparticle tended to aggregate together and act as the recombination centers, which could lead to the increase of recombination of photoexcited charges at Cu_2S nanoparticles. Therefore, the photoelectrochemical activity was gradually decreased when excess Cu_2S was deposited.

In order to study the photo-response of the TiO_2 NRs, TiO_2 BNRs, TiO_2 BNRs/CdS(9) and TiO_2 BNRs/CdS(9)/Cu_2S over time, the *I*–*t* curve of the materials at 0 V vs Ag/AgCl was measured. Fig. 12A indicated that the photocurrent density of all the measured samples in the dark was very low, very close to zero. However, upon the samples were illuminated with light, a transient photocurrent was produced due to the prompt effect of the excitation power, and the photocurrent maintained in a steady state. The results show that the photocurrent density of all the samples followed the order of TiO_2 NRs < TiO_2 BNRs < TiO_2 BNRs/CdS(9) < TiO_2 BNRs/CdS(9)/Cu_2S, which was consistent with the results presented in Figs. 8 and 9. The results further imply that the heterostructure formed between CdS and Cu_2S can promote the light utilization and efficient charge separation, leading to the rapid transfer of photosensitized electrons from Cu_2S to CdS, and then to TiO_2 branched nanorod arrays, which effectively prevents the recombination of electron–hole pairs and presents enhanced activity.

Furthermore, to measure the chemical stability of as-prepared solar PEC electrodes, linear sweep voltammogram was measured after C–V scanning for 1 and 100 cycles under illumination, and the experiments were also conducted in a three-electrode configuration. The TiO_2 BNRs/CdS(9)/Cu_2S(6) was used as the typical photoelectrodes. As shown in Fig. 12B, the photocurrent density of the material over 100 cycles was almost consistent to that over the first scan cycle, revealing an excellent capability to resist

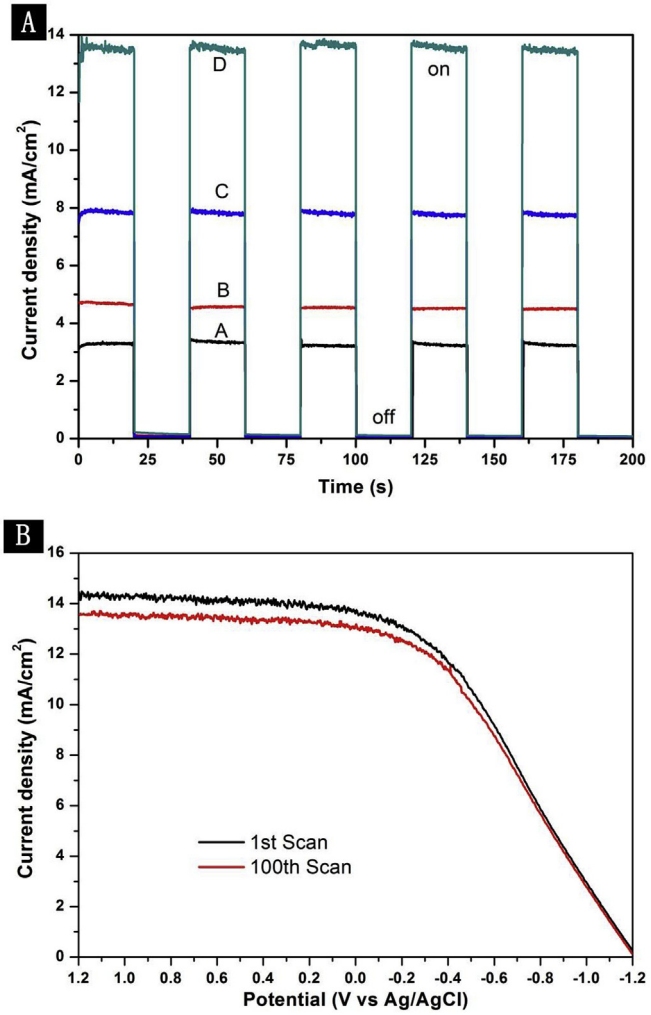

Fig. 12. (A) Photocurrent response of TiO_2 NRs, TiO_2 BNs, TiO_2 BNRs/CdS(9) and TiO_2 BNRs/CdS(9)/Cu_2S with on and off cycles. (B) Stability of TiO_2 BNRs/CdS(9)/Cu_2S after 100 scan.

photocorrosion.

4. Conclusion

In this work, TiO_2 branched nanorod arrays was synthesized, and CdS/Cu_2S heterostructure was successfully constructed on the surface of the TiO_2 BNRs by a facile two-step route via SILAR process. The effects of the CdS and Cu_2S SILAR cycles on the performance of the photoelectrode have been systematically investigated, and the optimal performance is found with 9 cycles of CdS and 6 cycles of Cu_2S deposition. As the existence of the heterostructure between TiO_2 and CdS, coupling with the heterostructure between CdS and Cu_2S, the synthesized TiO_2 BNRs/CdS/Cu_2S shows broadened absorption range in visible light, increased absorbance and remarkably enhanced photovoltaic performance, compared with bare TiO_2 BNRs and TiO_2 BNRs/CdS. The photocurrent density of TiO_2 BNRs/CdS(9)/Cu_2S(6) can reach to 13.65 mA cm^{-2} at a potential of 0 V versus Ag/AgCl, and the density is nearly two times and three times than that of pristine TiO_2 BNRs and TiO_2 BNRs/CdS(9), respectively. The CdS/Cu_2S not only extends the utilization of visible light, but also presents good photocorrosion resistance. In addition, the heterostructure between CdS and Cu_2S promotes charge injection from one semiconductor into another, which leads to efficient charge separation by reducing the recombination efficiency of the electron–hole pairs. The current work indicated that the TiO_2 BNRs/CdS/Cu_2S has great potential applications in the field of PEC water splitting and electrical devices. And formatting heterostructure of Cu_2S, CdS QDs and TiO_2 BNRs provides a promising way to fabricate materials applied in the PEC water splitting and solar energy conversion.

Acknowledgments

The study was financially supported by the National Program for Support of Top–Notch Young Professionals of China (2012), Projects 51222805, 51579096, 51521006, and 51508175 supported by National Natural Science Foundation of China, the Program for New Century Excellent Talents in University from the Ministry of Education of China (NCET–11–0129), Interdisciplinary Research Project of Hunan University, the Fundamental Research Funds for the Central Universities, Hunan University.

Appendix A. Supplementary data

Supplementary data related to this article can be found at http://dx.doi.org/10.1016/j.jallcom.2015.11.206

References

[1] H. Gao, J. Zhang, R. Wang, M. Wang, Appl. Catal. B Environ. 172-173 (2015) 1–6.
[2] Z. Xu, Y. Hongjian, W. Guopeng, M. Guijun, W. Fuyu, W. Lu, L. Can, J. Am. Chem. Soc. 130 (2008) 7176–7177.
[3] C.-H. Liao, C.-W. Huang, J.C.S. Wu, Catalysts 2 (2012) 490–516.
[4] M. Shao, F. Ning, M. Wei, D.G. Evans, X. Duan, Adv. Funct. Mater. 24 (2014) 580–586.
[5] S. Wenjun, S. Bo, S. Tielin, T. Xianhua, P. Zhengchun, L. Guanglan, ACS Nano 8 (2014) 7163–7169.
[6] Z. Braiek, A. Brayek, M. Ghoul, S. Ben Taieb, M. Gannouni, I. Ben Assaker, A. Souissi, R. Chtourou, J. Alloy Compd. 653 (2015) 395–401.
[7] B.E. Logan, S.-E. OH, I.S. Kim, S. Van Ginkel, Environ. Sci. Technol. 36 (2002) 2530–2536.
[8] D. Das, T. Veziroglu, Int. J. Hydrogen Energy 33 (2008) 6046–6057.
[9] Y. Liu, Y.-X. Yu, W.-D. Zhang, J. Phys. Chem. C 117 (2013) 12949–12957.
[10] A. Wolcott, W.A. Smith, T.R. Kuykendall, Y. Zhao, J.Z. Zhang, Small 5 (2009) 104–111.
[11] J.S. Zhong, Q.Y. Wang, Y.F. Yu, J. Alloy Compd. 620 (2015) 168–171.
[12] M.J. Kang, Y.S. Kang, J. Mater. Chem. A 3 (2015) 15723–15728.
[13] K. Sivula, R. Zboril, F.F. Le, R. Rosa, W. Anke, T. Jiri, F. Jiri, G. Michael, J. Am. Chem. Soc. 132 (2010) 7436–7444.
[14] K.-S. Ahn, S. Shet, T. Deutsch, C.-S. Jiang, Y. Yan, M. Al-Jassim, J. Turner, J. Power Sources 176 (2008) 387–392.
[15] V. Cristino, S. Caramori, R. Argazzi, L. Meda, G.L. Marra, C.A. Bignozzi, Langmuir 27 (2011) 7276–7284.
[16] N. Singh, S. Choudhary, S. Upadhyay, V.R. Satsangi, S. Dass, R. Shrivastav, J. Solid State Electr. 18 (2013) 523–533.
[17] F. Su, T. Wang, R. Lv, J. Zhang, P. Zhang, J. Lu, J. Gong, Nanoscale 5 (2013) 9001–9009.
[18] S. Hoang, S. Guo, N.T. Hahn, A.J. Bard, C.B. Mullins, Nano Lett. 12 (2012) 26–32.
[19] K. Guo, Z. Liu, C. Zhou, J. Han, Y. Zhao, Z. Liu, Y. Li, T. Cui, B. Wang, J. Zhang, Appl. Catal. B Environ. 154–155 (2014) 27–35.
[20] B. Liu, E.S. Aydil, J. Am. Chem. Soc. 131 (2009) 3985–3990.
[21] K.R. Moonoosawmy, M. Es-Souni, R. Minch, M. Dietze, M. Es-Souni, CrystEngComm 14 (2012) 474–479.
[22] S. Kuang, L. Yang, S. Luo, Q. Cai, Appl. Surf. Sci. 255 (2009) 7385–7388.
[23] W. Smith, A. Wolcott, R.C. Fitzmorris, J.Z. Zhang, Y. Zhao, J. Mater. Chem. 21 (2011) 10792.
[24] B. Sun, T. Shi, Z. Peng, W. Sheng, T. Jiang, G. Liao, Nanoscale Res. Lett. 8 (2013).
[25] Y.J. Hwang, C. Hahn, B. Liu, P. Yang, ACS Nano 6 (2012) 5060–5069.
[26] F. Su, J. Lu, Y. Tian, X. Ma, J. Gong, Phys. Chem. Chem. Phys. 15 (2013) 12026–12032.
[27] L. Tang, Y. Fang, Y. Pang, G. Zeng, J. Wang, Y. Zhou, Y. Deng, G. Yang, Y. Cai, J. Chen, Chem. Eng. J. 254 (2014) 302–312.
[28] L. Tang, G.-D. Yang, G.-M. Zeng, Y. Cai, S.-S. Li, Y.-Y. Zhou, Y. Pang, Y.-Y. Liu, Y. Zhang, B. Luna, Chem. Eng. J. 239 (2014) 114–122.
[29] L. Tang, S. Zhang, G.M. Zeng, Y. Zhang, G.D. Yang, J. Chen, J.J. Wang, J.J. Wang, Y.Y. Zhou, Y.C. Deng, J. Colloid Interface Sci. 445 (2015) 1–8.
[30] Y. Zhou, L. Tang, G. Zeng, J. Chen, Y. Cai, Y. Zhang, G. Yang, Y. Liu, C. Zhang, W. Tang, Biosens. Bioelectron. 61 (2014) 519–525.
[31] I.S. Cho, Z. Chen, A.J. Forman, D.R. Kim, P.M. Rao, T.F. Jaramillo, X. Zheng, Nano

Lett. 11 (2011) 4978–4984.
[32] J.S. Yang, W.P. Liao, J.J. Wu, ACS Appl. Mater Interfaces 5 (2013) 7425–7431.
[33] J. Liu, X. Yu, Q. Liu, R. Liu, X. Shang, S. Zhang, W. Li, W. Zheng, G. Zhang, H. Cao, Z. Gu, Appl. Catal. B Environ. 158–159 (2014) 296–300.
[34] P. Fu, P. Zhang, Appl. Catal. B Environ. 96 (2010) 176–184.
[35] H. Cao, Z. Wang, G. Hou, G. Zheng, Surf. Coat. Tech. 205 (2010) 885–889.
[36] J. Zhuang, Q. Tian, H. Zhou, Q. Liu, P. Liu, H. Zhong, J. Mater. Chem. 22 (2012) 7036.
[37] K. Nishijima, B. Ohtani, X. Yan, T.-a. Kamai, T. Chiyoya, T. Tsubota, N. Murakami, T. Ohno, Chem. Phys. 339 (2007) 64–72.
[38] Y. Cui, H. Du, L. Wen, Solid State Commun. 149 (2009) 634–637.
[39] C. Cao, C. Hu, W. Shen, S. Wang, Y. Tian, X. Wang, J. Alloy Compd. 523 (2012) 139–145.
[40] K. Anil, J.A. Kumar, J. Mol. Catal. Chem. 165 (2001) 265–273.
[41] Q. Liu, H. Lu, Z. Shi, F. Wu, J. Guo, K. Deng, L. Li, ACS Appl. Mater Interfaces 6 (2014) 17200–17207.
[42] P. Lv, W. Fu, Y. Mu, H. Sun, S. Su, Y. Chen, H. Yao, D. Ding, T. Liu, J. Wang, H. Yang, J. Alloy Compd. 621 (2015) 30–34.
[43] Z. Li, L. Yu, Y. Liu, S. Sun, Electrochim. Acta 129 (2014) 379–388.
[44] M. Li, Y. Liu, H. Wang, H. Shen, W. Zhao, H. Huang, C. Liang, J. Appl. Phys. 108 (2010) 094304.
[45] M. Savelli, J. Bougnot, Solar Energy Convers. 31 (1979) 213–256.
[46] G. Liu, T. Schulmeyer, A. Thissen, A. Klein, W. Jaegermann, Appl. Phys. Lett. 82 (2003) 2269.
[47] S.C. Riha, S. Jin, S.V. Baryshev, E. Thimsen, G.P. Wiederrecht, A.B. Martinson, ACS Appl. Mater Interfaces 5 (2013) 10302–10309.
[48] Y. Bessekhouad, R. Brahimi, F. Hamdini, M. Trari, J. Photoch. Photobiol. A Chem. 248 (2012) 15–23.
[49] Y. Chen, Z. Qin, X. Wang, X. Guo, L. Guo, RSC Adv. 5 (2015) 18159–18166.
[50] Z. Liu, G. Ji, D. Guan, B. Wang, X. Wu, J. Colloid Interface Sci. 457 (2015) 1–8.
[51] L. Yu, Z. Li, Y. Liu, F. Cheng, S. Sun, J. Mater. Sci. Mater. Electr. 26 (2015) 2286–2295.
[52] N.K. Allam, C.A. Grimes, Sol. Energy Mat. Sol. C 92 (2008) 1468–1475.
[53] S.U.M. Khan, M. Al-Shahry, W.B. Ingler, Science 297 (2002) 2243–2245.
[54] J. Luo, L. Ma, T. He, C.F. Ng, S. Wang, H. Sun, H.J. Fan, J. Phys. Chem. C 116 (2012) 11956–11963.
[55] Z. Xie, X. Liu, W. Wang, C. Liu, Z. Li, Z. Zhang, Sci. Technol. Adv. Mat. 15 (2014) 055006.
[56] W. Yue, W. Cyrus, M. Wanli, S. Bryce, A.A. Paul, A.A. Paul, Nano Lett. 8 (2008) 2551–2555.